Frequency-specific directed interactions in the human brain network for language

Jan-Mathijs Schoffelen[a,b,1], Annika Hultén[a,b,2], Nietzsche Lam[a,b], André F. Marquand[a], Julia Uddén[a,b,3], and Peter Hagoort[a,b,1]

[a]Radboud University Nijmegen, Donders Institute for Brain, Cognition, and Behaviour, 6500 HB Nijmegen, The Netherlands; and [b]Max Planck Institute for Psycholinguistics, 6525 XD Nijmegen, The Netherlands

Edited by Barry Giesbrecht, University of California, Santa Barbara, CA, and accepted by Editorial Board Member Michael S. Gazzaniga June 8, 2017 (received for review February 23, 2017)

The brain's remarkable capacity for language requires bidirectional interactions between functionally specialized brain regions. We used magnetoencephalography to investigate interregional interactions in the brain network for language while 102 participants were reading sentences. Using Granger causality analysis, we identified inferior frontal cortex and anterior temporal regions to receive widespread input and middle temporal regions to send widespread output. This fits well with the notion that these regions play a central role in language processing. Characterization of the functional topology of this network, using data-driven matrix factorization, which allowed for partitioning into a set of subnetworks, revealed directed connections at distinct frequencies of interaction. Connections originating from temporal regions peaked at alpha frequency, whereas connections originating from frontal and parietal regions peaked at beta frequency. These findings indicate that the information flow between language-relevant brain areas, which is required for linguistic processing, may depend on the contributions of distinct brain rhythms.

language | Granger causality | brain networks | magnetoencephalography

The human brain is capable of effortlessly extracting meaning from sequences of written or spoken words by means of a sophisticated interplay between dedicated neocortical regions. Neuroanatomical research has revealed a number of white-matter pathways that facilitate these interregional interactions (1). Electrophysiological research with electro- and magnetoencephalography (EEG/MEG) has revealed with high temporal precision the sequential activation of individual nodes embedded within the human brain network for language (2, 3). However, the nature of the functional interactions that enable the efficient flow of information between the nodes of this network has yet to be elucidated.

One important feature of cortical interregional connections is that they are frequently reciprocal in nature (4), which implies that information can be exchanged in a bidirectional fashion. Moreover, the information flow between cortical regions may be facilitated by interregional rhythmic synchronization (5), where neuronal rhythms of specific different frequencies reflect the direction in which the information is flowing (6, 7). This bidirectional flow of information should also be a crucial feature of the neurobiological system that supports language processing. Linguistic processing is not a simple bottom-up process where incoming linguistic information (for instance, when reading a sentence) drives a sequence of activations of cortical areas that gradually transforms a string of letters into a representation of sentence and discourse meaning. Rather, contextual information, which is either already available, or built up while a sentence unfolds, can also provide top-down information, affecting the response in lower-order areas.

Here, we show that interregional interactions in the human brain network for language are subserved by rhythmic neuronal synchronization at specific frequencies. Specifically, we found that rhythmic activity in the alpha frequency range (8–12 Hz) propagates from temporal cortical areas to frontal cortical areas, and that beta frequency rhythmic activity (15–30 Hz) propagates in the opposite direction. These results indicate the functional relevance of rhythmic directed interactions during language processing, where interactions between areas are supported by different frequency bands, depending on the direction of the interaction. This functional relevance likely extends to other cognitive domains, reflecting a generic mechanism that allows for dynamic routing of information in a network of task-relevant brain regions.

Results

We used MEG to record neuromagnetic signals while participants were reading sequences of words. We reconstructed the cortical activity in a set of predefined brain areas (consisting of 156 cortical parcels), encompassing areas that are part of the core language system, areas in the visual system, and homolog areas in the contralateral hemisphere (8) (Fig. 1*A*). Next, we computed frequency-resolved Granger causality (GC) to quantify directed rhythmic neuronal interactions between brain areas for language that are known to be anatomically connected (9–11). Because the interpretation of connectivity estimated from neuromagnetic recordings is highly confounded by spatial leakage of source activity (12), we statistically compared, across the sample of 102 participants, the estimated GC with an estimate of GC after time reversal of the signals (13). This allowed us to conservatively discard a substantial subset of the predefined connections for which the direction and/or the strength of the estimated Granger causal interaction is likely

Significance

The brain's remarkable capacity for language requires bidirectional interactions between functionally specialized brain regions. Although the functional role of individual regions in the brain network for language has been well studied, as of yet little is known about the mechanisms that facilitate the information exchange between these brain regions. In this paper we show that communication between language-relevant areas in the brain is supported by rhythmic neuronal synchronization and that different rhythms reflect the direction of information flow. These findings likely reflect a generic mechanism that allows for dynamic routing of information in a network of task-relevant brain regions during cognitive processing.

Author contributions: A.H., J.U., and P.H. designed research; J.-M.S., A.H., N.L., and J.U. performed research; J.-M.S. contributed new reagents/analytic tools; J.-M.S. and A.F.M. analyzed data; J.-M.S. and P.H. wrote the paper; and A.H., N.L., and A.F.M. helped with part of the analysis.

The authors declare no conflict of interest.

This article is a PNAS Direct Submission. B.G. is a guest editor invited by the Editorial Board.

[1]To whom correspondence may be addressed. Email: j.schoffelen@donders.ru.nl or p.hagoort@donders.ru.nl.

[2]Present address: Department of Neuroscience and Biomedical Engineering, Aalto University, FI-00076 Helsinki, Finland.

[3]Present address: Department of Linguistics and Stockholm University Brain Imaging Centre, University of Stockholm, SE-106 91 Stockholm, Sweden.

This article contains supporting information online at www.pnas.org/lookup/suppl/doi:10.1073/pnas.1703155114/-/DCSupplemental.

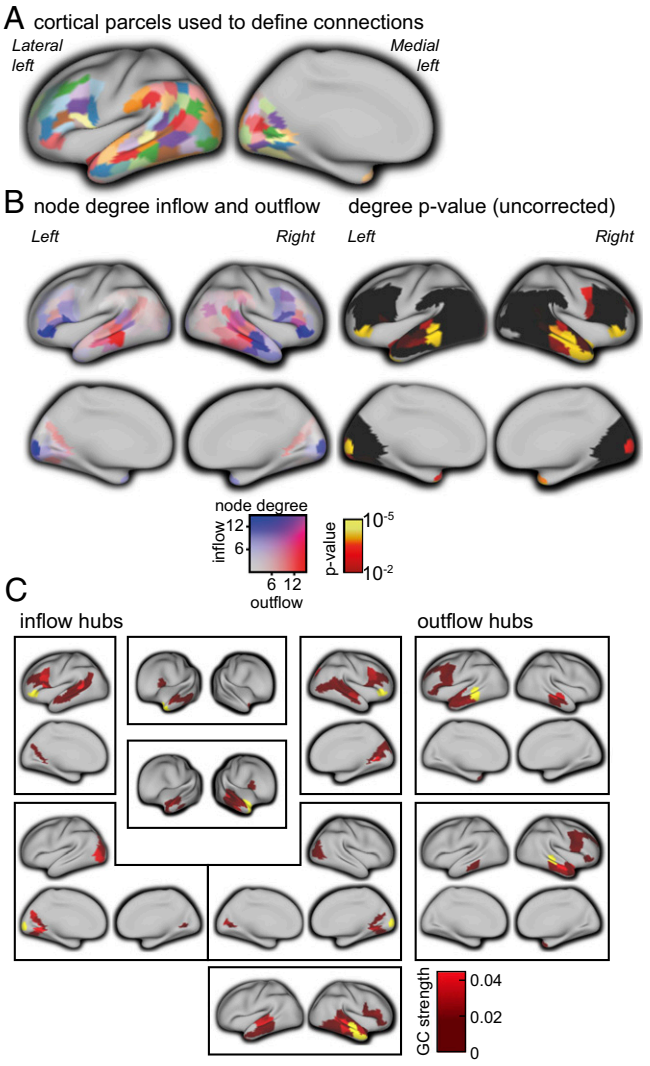

Fig. 1. Topology of the brain network for language as quantified with GC. (*A*) Overview of the left hemispheric anatomical parcels used for source reconstruction and serving as network nodes, displayed on the inflated cortical surface. Lateral and medial surfaces are shown on the *Left* and *Right*, respectively. Right hemispheric homologous parcels were also considered for network estimation, yet not displayed here. (*B*, *Left*) Node degree for inflow (i.e., the number of nodes from which each of the nodes receives significant Granger causal input) ($P < 0.05$, nonparametric permutation test, Bonferroni corrected) and outflow (i.e., the number of nodes to which each of the nodes sends significant Granger causal output). (*B*, *Right*) Uncorrected *P* values associated with the statistical comparison (nonparametric permutation) of the topology observed in the left panels, and randomly connected networks, keeping the overall degree distribution constant. Orange/yellow parcels survive Bonferroni correction for multiple comparisons (the number of edges) and reflect hubs in the network. (*C*) Topology of the connections for each of the highly connected hubs identified in *B*, and the other cortical areas, for inflow hubs (blue parcels in *B*) and outflow hubs (red parcels in *B*), with the hubs displayed in yellow, and the Granger causal strength to sending/receiving areas in red.

confounded by spatial leakage of activity. This left us with a subset of 713 connections from the initial 4,350 connections formed between 156 modeled cortical parcels. We subsequently explored the topology of the resulting network and observed an uneven distribution in the number of connections for the cortical parcels involved (Fig. 1 *B* and *C*). Specifically, for each of the cortical parcels we quantified the number of in- and outgoing directed connections (i.e., the node degree). We observed left and right middle temporal cortical parcels to serve as a sender node in a large number of connections, projecting to ipsilateral anterior middle and superior temporal cortex [Brodmann areas (BA) 21/22/38], to contralateral middle and superior temporal cortex (BA 21/22), and to frontal cortex (BA 6/9/44/45/47) ($P < 0.05$, Bonferroni corrected randomization test). Left and right inferior frontal regions (BA 47), however, were observed to receive Granger causal input from ipsilateral frontal cortex (BA 44/45/46), ipsilateral superior temporal cortex (BA 22), ipsilateral angular gyrus (BA 39), and ipsilateral extrastriate visual cortex (BA 19, area 17/18 present in the right hemisphere only) ($P < 0.05$, Bonferroni corrected randomization test). Additionally, regions receiving substantial inflow were located bilaterally in the anterior temporal pole (receiving input from superior and middle temporal regions, as well as from inferior frontal cortex), in the occipital pole (receiving input from extrastriate regions as well as from inferior temporal and occipito-temporal cortex), and in the right anterior temporal cortex.

To gain more detailed insight into the spatial and spectral structure of this brain wide network we applied nonnegative matrix factorization (NMF) to the group-level connectivity data (8). Specifically, we modeled the connectivity data as a mixture of a limited number of spatially static network components, each with a subject-specific spectral profile. The decomposition algorithm did not incorporate any specific constraints with respect to the spatial or spectral structure of the underlying components. In particular, no assumptions were made about the spatial clustering of edges (i.e., the decomposition algorithm did not favor sets of connections to end up in the same component when the cortical parcels on each end of the directed connection were spatially clustered). However, the majority of extracted network components were physiologically interpretable, judging from the spatial clustering of the cortical parcels participating in component-specific directed interactions. Fig. 2 shows the network components with predominant connections between language-relevant cortical areas (components with predominant connections between visual cortical areas and components with more spatially diffuse connections are shown in Fig. S1). The components' cortical locations for outflow and inflow are depicted in blue and orange/yellow, respectively, in the leftmost panel for each quadruplet of columns. For some of the components, the subject-averaged spectral profiles were band-limited to a certain frequency range, which moreover showed a consistent peak frequency across subjects (Fig. 2 *B–H*, middle panels for each quadruplet of columns). This suggests that these components represent frequency-specific rhythmic directed interactions between key regions in this large-scale network. We categorized the extracted components based on the dominant region for outflow. The majority of the components reflected predominantly intrahemispheric connections (Fig. 2 *B–H*, right panel for each quadruplet of columns). We identified left and right hemispheric directed rhythmic interactions from posterior and midtemporal cortical regions to ipsilateral frontal cortex (mainly inferior frontal), with a median peak frequency at 12 Hz [interquartile range (IQR) 11–13 Hz] (Fig. 2*B*). A somewhat spatially more diffuse component with predominantly left intrahemispheric connections led from midtemporal areas to inferior and superior frontal areas (Fig. 2*C*). Connections from posterior and midtemporal regions to ipsilateral anterior temporal cortex had a slightly higher median peak frequency of 14 Hz (with an IQR of 12–15 Hz and 13–15 Hz for the left and right hemispheric components), compared with the temporo-frontal connections (Fig. 2*D*). Next, there was a set of components predominantly interconnecting temporal cortical regions that showed somewhat more variability in their spectral profile across subjects (Fig. 2*E*). These components reflected connections from superior and middle temporal cortex (along the whole anterior–posterior axis) to mid and anterior inferior temporal cortex, and connections from midmiddle and superior anterior temporal cortex to the temporal pole.

In contrast to the network components with the outflow regions in temporal cortex, the rhythmic interactions with predominant

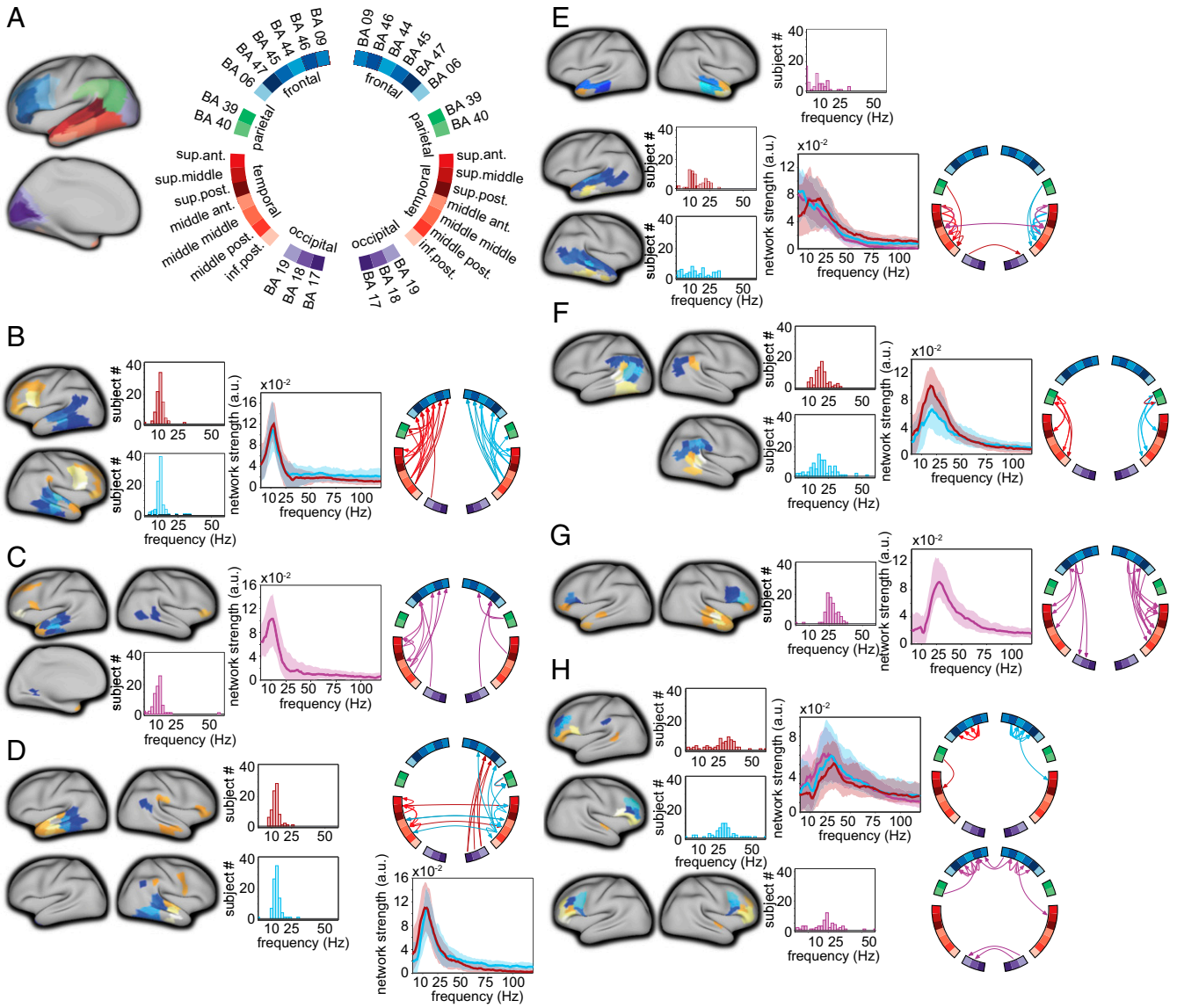

Fig. 2. Network components obtained with NMF show frequency, regional, and direction-specific interactions. (*A*) Location of the cortical nodes, displayed on an inflated cortical sheet (*Left*) with color coding and labeling convention (*Right*), as used in *B–H*. Circular grouping was according to anatomical location, using BA labeling for the parcels outside temporal cortex, and using their relative location along the anterior/posterior and superior/inferior axis for temporal parcels. (*B–H*) Components reflecting connections between language-relevant cortical areas. Leftmost panels show the location of the parcels involved. Dark/light blue colors: regions for outflow (the lighter the color of the parcel, the stronger the relative contribution of the parcel to the component). Orange/yellow/white colors: regions for inflow. The histograms show for each of the components the distribution of the subject-specific peak frequency. The spectra show the median (and IQR) spectral profiles across subject. The circular plots show the directed connections between the parcels. The thickness of the arrows reflects the relative strength of the connection. Components with predominantly left-hemispheric, right-hemispheric, or bilateral connections are displayed in red, light blue, and purple, respectively. (*B*) Left and right hemispheric components from temporal regions to ipsilateral frontal regions. (*C*) Component with bilateral intrahemispheric temporal-to-frontal connections. (*D*) Left and right hemispheric components with predominant connections from middle to anterior temporal regions. (*E*) Components with predominantly intratemporal connections from superior to inferior regions (upper two rows), and from midanterior regions to the temporal pole (bottom row). (*F*) Components with predominant connections from the angular gyrus (BA 39) and supramarginal gyrus (BA 40) to posterior temporal cortex. (*G*) Component from frontal regions to temporal regions. (*H*) Components with predominantly fronto-frontal connections.

outflow from parietal (Fig. 2*F*) and frontal (Fig. 2 *G* and *H*) regions consistently showed a higher peak frequency of interaction. Components reflecting parietal-to-posterior temporal interactions had a median peak frequency of 20 Hz (with an IQR of 17–22 Hz and 15–26 Hz for the left and right hemispheric components, respectively) and frontal-to-temporal rhythmic interactions had a median peak frequency of 27 Hz (with an IQR of 25–30 Hz). Intrafrontal interactions had a somewhat more broadband spectral profile, with a median peak frequency of 24 Hz (IQR: 19–29 Hz) for directed interactions from BA 44 to BA 45/46/47. Interactions from BA 46 to BA 44/45/47 had a median peak frequency of 30 Hz (IQR: 23–35 Hz) and 29 Hz (IQR: 25–33 Hz) for left and right hemispheric connections, respectively. We statistically evaluated the peak frequency of the rhythmic interactions between components with predominant connections between parietal, frontal, and temporal brain areas (Fig. 3*A*). Overall, the component-specific median peak frequencies ranged from the upper end of the alpha range (12 Hz) to the upper end of the beta range (30 Hz). Moreover, components with rhythmic Granger causal outflow predominantly from temporal areas had a consistently lower peak

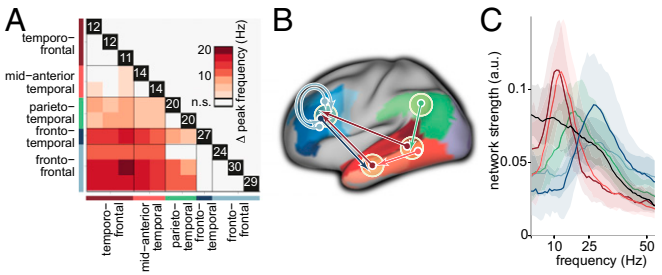

Fig. 3. Rhythmic interactions originating from temporal/parietal cortex have consistently lower peak frequencies than those originating from frontal cortex. (*A*) Pairwise comparison of the component-specific peak frequencies (nonparametric permutation test, corrected for multiple comparisons). Each colored element represents the median of the subject-specific difference in peak frequency (row component – column component). The values in the black boxes along the main diagonal reflect the median peak frequency for each component. (*B*) Schematic representation of the directed rhythmic cortico-cortical interactions in the language system, grouped according to the cortical output area. The temporal lobe is split into two "nodes," to be able to display the rhythmic mid to anterior connection. The colored arrows refer to the spectra shown in *C*. The black spectrum in *C* is the average of the components shown in (Fig. 2*E*), with dominant connections from superior temporal to middle temporal gyrus, and is not displayed as a separate connection in *B*.

frequency than components with Granger causal outflow from parietal or frontal areas ($P < 0.05$, nonparametric permutation test, multiple comparison corrected). Notably, based on the NMF we could distinguish temporo-frontal interactions, with a peak frequency of 12 Hz (Figs. 2 *A* and *B* and 3 *B* and *C*, connection in dark red), from fronto-temporal interactions, with a peak frequency of 27 Hz (Figs. 2*F* and 3 *B* and *C*, connection in dark blue). Fig. 3*B* shows a schematic summary of the dominant rhythmic interactions, with the corresponding spectral profile in Fig. 3*C*.

We proceeded to test whether the strength of the rhythmic interactions was modulated by the functional requirements imposed by the perceptual input. To this end, we divided the stimulus material into four conditions, based on whether the subjects were reading a well-structured sentence or a pseudorandom sequence of words (sentences and word lists), and based on the ordinal position of the words (early and late words). Importantly, we stratified the data for lexical frequency and overall signal variance, to avoid as much as possible interpretational confounds for the estimated connectivity (12, 14) due to differences in univariate signal and stimulus properties (8). Subsequently we computed the Granger causal interactions for each subject and condition for the most prominent functional connections, which were extracted from the NMF results by means of spatial clustering. We constrained the analysis to band-limited estimates of GC, averaging across frequencies and edges. The connection-specific frequency bands were obtained from the components' peak frequencies and IQRs. Contrasting sentences with sequences, we observed the strength of the interactions to be modulated from left middle temporal regions to the left temporal pole, where sequences elicited stronger interactions than sentences, and from right striate to extrastriate visual regions (Fig. 4*A*, $P < 0.05$, nonparametric permutation test, Holm–Bonferroni correction for multiple comparisons). Comparing early words with late words in the sentence condition showed several significantly modulated connections, with rhythmic interactions being stronger early in the sentence (Fig. 4*B*). These connections were bilateral from temporal to frontal regions, and from middle temporal regions to the temporal pole. In addition, in the right hemisphere we identified significantly modulated connections from frontal regions to temporal regions, and from the superior temporal gyrus to the middle temporal gyrus ($P < 0.05$, nonparametric permutation test, Holm–Bonferroni correction for multiple comparisons). Moreover, we identified two right hemispheric connections that showed a significant interaction effect between early vs. late words and sentences vs. sequences (Fig. 4*B* and Fig. S2).

Discussion

We have provided evidence for directed interactions between cortical regions in the human brain network for language during sentence reading. Topological analysis of the overall network revealed a high degree of Granger causal inflow into anterior inferior frontal cortical regions, right anterior temporal cortex, and the temporal pole bilaterally. This is in line with these regions' being "high-order" regions, involved in the processing of more abstract features of the linguistic input, which requires integration of converging information. Frontal regions are engaged in unification operations (15), integrating lexical units into the larger context. Anterior temporal cortex is associated with conceptual object representations (16, 17).

Middle temporal cortical regions, however, displayed a high degree of Granger causal outflow. This is in agreement with the middle temporal gyrus' crucial role in language comprehension at the level of single words (18, 19). Its functional connections to more anterior temporal areas, as well as to inferior frontal cortex, reflect the necessity to propagate information about individual lexical items to areas that subserve integration operations. Notably, we did not observe a clear lateralization in the pattern of connections, which lends support to the evolving notion that both cerebral hemispheres are involved in the processing of linguistic stimuli (20).

Data-driven decomposition of the overall network into smaller subnetworks revealed several spatially constrained components, corresponding with local and long-range directed interactions. The clear frequency-resolved profile displayed by some of these components displayed is indicative of the interactions' being mediated by rhythmic interareal synchronization. Connections originating from temporal cortical areas showed a consistently lower peak frequency (alpha and low beta) than connections originating from parietal or

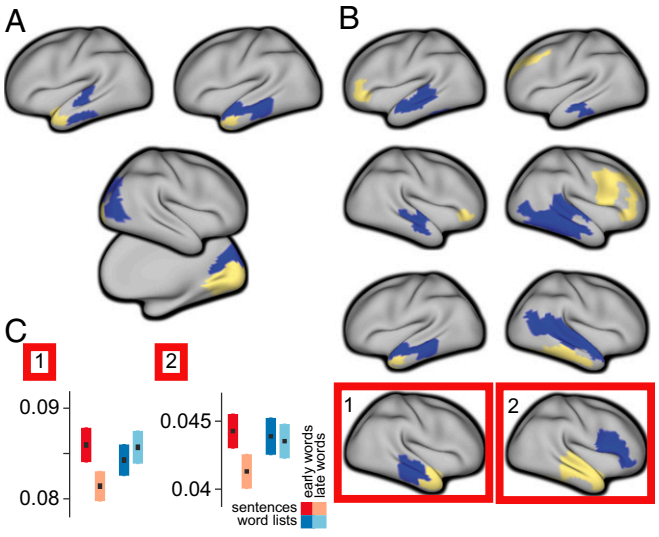

Fig. 4. The strength of directed interactions is modulated by the linguistic input. (*A*) Connections showing stronger interactions in the word list condition than in the sentence condition ($P < 0.05$, corrected Bonferroni–Holm). Blue parcels indicate nodes for outflow and yellow parcels indicate nodes for inflow. (*B*) Connections showing stronger interactions for early words in the sentences, compared with late words in the sentences. The connections shown in the red boxes show a significant interaction effect ($P < 0.05$, corrected), on top of a significant early vs. late effect. (*C*) Bar graphs show condition-specific mean (±SEM) Granger causal strength for the outlined connections.

frontal regions (high beta). As a specific example, temporal-to-frontal interactions are subserved by rhythmic synchronization at ∼12 Hz, whereas interactions in the opposite direction, from frontal to temporal regions, peak at a frequency of ∼27 Hz.

At first glance, these findings correspond well with recent work in the visual system in which it was shown that feedforward and feedback connections, as defined by their characteristic cortical laminar connectivity profile (21), could be distinguished in terms of their frequency of interaction (6, 7, 22). However, in the visual system, feedforward connections have been functionally characterized by gamma band synchronization (>50 Hz) (and to a lesser extent by theta band synchronization) and feedback connections by alpha/beta synchronization. A GC spectral peak in the gamma frequency range was absent in our data. Although studies in the visual system allow for experimental paradigms eliciting robust and strongly modulated gamma band rhythmicity, language paradigms do not typically lead to similarly strong local gamma-band responses (23), rendering the likelihood of detecting gamma-band interactions low. In addition, characterization of feedforward and feedback connections based on their cytoarchitectonic connectivity profiles is likely to be more distinct in peripheral sensory systems than in higher cortical regions (24), such as the higher-order areas in the human brain network for language. Consequently, there is no reason to assume that the emergent functional properties of the language network, in terms of the frequency of interactions, should directly map onto observations in the visual system. Nevertheless, our data reveal frequency-specific subnetworks in the brain system for language.

Further exploration of the potential functional significance of these interactions revealed that the linguistic context modulates left lateralized midtemporal-to-anterior temporal interactions, as well as right lateralized extrastriate-to-striate interactions. In these connections, Granger causal influences were stronger in the word list condition. This suggests that the absence of syntactic structure intensifies the need for information transfer to the anterior temporal lobe, possibly to facilitate access to word meaning. In addition, our findings indicate that even the generation of a word form percept might require stronger interactions for effective processing in the absence of context constraining syntactic structure. Next, in a sentential context, the incremental availability of contextual information allows for the generation of constraining predictions about the upcoming input, likely facilitating processes such as lexical selection. Bilateral interactions from temporal to frontal regions, from midtemporal to anterior temporal regions, from right lateralized frontal to temporal regions, and from superior temporal to middle temporal regions are stronger early in the sentence, when the constraining context is still relatively weak, as opposed to later in the sentence. These stronger interactions early in the sentence might reflect the increased need for information exchange between these regions, to establish a linguistic context.

In conclusion, this study shows directional interactions in the highly dynamic cortical network of language-relevant areas, with salient differences in the specific frequencies that support the communication protocols in the temporo-frontal and the fronto-temporal directions. Although our findings are in line with earlier reports of a frequency difference between feedforward and feedback connections, the carrier frequencies in the language network shown here deviate from what has been observed in the visual system. However, the effect of linguistic context on the strength of some of these connections suggests the functional relevance of dynamic rhythmic cortical interactions during cognitive processing in general, and language processing in particular (25). An interesting avenue for further research would be to relate these rhythmic interactions to local measures of activation, to gain insight into how the interplay between local cortical activity and long-range interactions shapes cognition.

Materials and Methods

Experimental Procedure and MEG Data Acquisition. Native Dutch speakers (n = 102, 51 males), with an age range of 18–33 y, participated in the experiment. All participants were right-handed, had normal or corrected-to-normal vision, and reported no history of neurological, developmental, or language deficits. The study was approved by the local ethics committee (CMO, the local "Committee on Research Involving Human Participants" in the Arnhem–Nijmegen region) and followed the guidelines of the Helsinki declaration. All participants gave written informed consent before participation. The participants read sequences and lists of words (total number of 240, with 9–15 words per sequence), presented sequentially on a back-projection screen, placed in front of them. MEG data were collected with a sampling frequency of 1,200 Hz. Throughout the measurement the head position was continuously monitored using custom software (26).

Artifact Rejection and Subtraction of Single-Trial Activity. All analyses were done with custom-written MATLAB scripts and FieldTrip (27). Data were epoched from −100 to 600 ms relative to word onset, and segments contaminated by artifacts were discarded before further analysis. We subtracted the event-related response from the single-trial data with the ASEO algorithm (28), aiming to attenuate the effects of evoked transients on the estimation (and subsequent interpretation) of GC (29). Transients in the signals violate the underlying assumption of stationarity and result in nonzero GC estimates, due to systematic latency differences of the peak of the transient signals across regions. We combined the ASEO algorithm with a blind source separation technique [denoising source separation (DSS) (30)]. We modeled single-trial signals as a combination of ongoing activity and event-related components (31) and subtracted the modeled single-trial evoked responses from the data (Fig. S3).

Source Reconstruction and Parcellation of Source-Reconstructed Activity. We performed source reconstruction using a linearly constrained minimum variance beamformer (LCMV) (32), estimating a spatial filter at 8,196 locations of the subject-specific reconstructed midcortical surface. Next, we applied an atlas-based parcellation scheme to reduce the dimensionality of the data. We used a refined version the Conte69 atlas, resulting in a parcellation scheme consisting of 191 parcels per hemisphere. Spatial filters were concatenated across vertices comprising a parcel, and we obtained a set of time courses of the event-related field at each parcel and selected for each parcel the first two spatial components explaining most of the variance in the signal. We opted for this method, rather than averaging, because we used rank-reduced forward solutions (excluding the most noise-sensitive dipole orientations), which might result in signal cancellation effects upon averaging, due to sign ambiguity of the resulting cardinal dipole orientations.

Preselection of the Connections Between Language-Relevant Areas. We constrained ourselves a priori to a subset of connections between parcel pairs, using known "long-range" macroanatomical fiber pathways between parcels comprised of core language regions and the visual system as described in the literature (1, 9–11). In addition, we allowed a priori for direct connections between neighboring nodes, based on the characteristics of cortico-cortical connections (e.g., refs. 24 and 33). We included intrahemispheric connections from both hemispheres and also included interhemispheric connections between homologous areas. Fig. 2*A* shows how the individual nodes were labeled. Connections between directly adjacent parcels were excluded for further analysis to reduce spurious estimates of connectivity due to spatial leakage of source-reconstructed activity. The selection scheme resulted in 4,350 connections between pairs of parcels, which notably consisted of a sparse subset of all possible pairwise connections between the 156 parcels used for the GC analysis.

GC Computation and Statistical Evaluation of Overall Network Topology. We computed the spectral representation of the signals at the sensor level and projected this into source space, using the parcel-specific spatial filters. The spectral representation of the signals was obtained using the fast Fourier transform in combination with multitapers (using 5-Hz smoothing) on the time domain data from 200 until 600 ms after word onset. For each pair of parcels we computed the cross-spectral density matrix and used this to compute GC using nonparametric spectral matrix factorization and a blockwise approach (34, 35). We also computed GC based on the source-projected Fourier transform of time-reversed data, to distinguish "weak" asymmetries from "strong" asymmetries, as described by Haufe and coworkers (13) and Haufe et al. (36). A weak asymmetry is an apparent directional interaction between a pair of network nodes, which is due to a difference in signal-to-noise ratio (SNR) across nodes (14), often caused by a linear mixture of underlying sources (37). We selected only parcel pairs for subsequent analysis for which the difference

between GC and reverse GC was statistically significant (across subjects) at a P value <0.05, corrected for multiple comparisons (one-sided t test, with Bonferroni correction). This reduced the number of connections that were used for subsequent analysis from 4,350 to 713.

NMF and Network Visualization. We explored the network topology by performing NMF with sparsity constraints (38) on the resulting GC spectra. The purpose of this analysis is to describe the reconstructed connectivity data as a low-dimensional mixture of network components, each of which with a subject–specific spectral profile. This technique has successfully been applied to sensor-level MEG-signals before (39). We opted for sparse NMF, because the nonnegativity constraint facilitates the interpretation of the components, as opposed to, for example, a statistical independence constraint as applied in independent component analysis. This is because GC is strictly nonnegative. The outcome of NMF is dependent on the number of components. We explored a range of "number of components" but settled on the number 20 for the remainder of the paper, providing a reasonable balance between providing a small number of interpretable components, while at the same time maintaining a good separation between subnetworks. We used the Icasso framework (40), with 40 repeated random initialization, which applies a hierarchical clustering procedure on the outcome to extract the underlying structure of the data, irrespective of the random initializations of the NMF algorithm.

Condition-Specific Statistical Evaluation. We estimated condition-specific GC in the dominant connections extracted from the identified network components. The individual conditions were defined according to whether the words were presented in a well-formed sentence context (or were part of a word list) and according to whether the words were presented early in the sentence/word list (words two to four) or late in the sentence/word list ($n-3$ until $n-1$, with n the number of words in the sentence/word list). To account for potential interpretational confounds of the resulting GC estimates we used a stratification procedure to ensure that the marginal distributions of the epochwise signal variances as well as the words' lexical frequencies were equalized across conditions. As a consequence only a subset of epochs is used for the GC estimation, where the parcel-pair specific number of epochs varies across parcel pairs. On average 50% of the epochs were retained (range: 20–75%), corresponding to 147 (range: 45–235) epochs. We defined dominant connections as spatially clustered sets of edges. We computed subject- and condition-specific GC and performed a nonparametric permutation test to evaluate (*i*) sentence – word list words, (*ii*) for the sentence condition: early – late words, and (*iii*) an interaction effect: (early-late words sentences) – (early-late words sequences).

ACKNOWLEDGMENTS. This work was supported by a Dutch Organization for Scientific Research (NWO) gravitation grant and Spinoza award (to P.H.) and an NWO VIDI grant (to J.-M.S.).

1. Dick AS, Bernal B, Tremblay P (2014) The language connectome: New pathways, new concepts. *Neuroscientist* 20:453–467.
2. Marinkovic K, et al. (2003) Spatiotemporal dynamics of modality-specific and supramodal word processing. *Neuron* 38:487–497.
3. Salmelin R, Helenius P, Service E (2000) Neurophysiology of fluent and impaired reading: A magnetoencephalographic approach. *J Clin Neurophysiol* 17:163–174.
4. Markov NT, et al. (2013) Cortical high-density counterstream architectures. *Science* 342:1238406.
5. Fries P (2015) Rhythms for cognition: Communication through coherence. *Neuron* 88: 220–235.
6. Bastos AM, et al. (2015) Visual areas exert feedforward and feedback influences through distinct frequency channels. *Neuron* 85:390–401.
7. Michalareas G, et al. (2016) Alpha-beta and gamma rhythms subserve feedback and feedforward influences among human visual cortical areas. *Neuron* 89:384–397.
8. Schoffelen J-M, Oostenveld R, Fries P (2005) Neuronal coherence as a mechanism of effective corticospinal interaction. *Science* 308:111–113.
9. Glasser MF, Rilling JK (2008) DTI tractography of the human brain's language pathways. *Cereb Cortex* 18:2471–2482.
10. Catani M, et al. (2007) Symmetries in human brain language pathways correlate with verbal recall. *Proc Natl Acad Sci USA* 104:17163–17168.
11. Friederici AD (2009) Pathways to language: Fiber tracts in the human brain. *Trends Cogn Sci* 13:175–181.
12. Schoffelen J-M, Gross J (2009) Source connectivity analysis with MEG and EEG. *Hum Brain Mapp* 30:1857–1865.
13. Winkler I, Panknin D, Bartz D, Müller K-R, Haufe S (2016) Validity of time reversal for testing Granger causality. *IEEE Trans Signal Process* 64:2746–2760.
14. Bastos AM, Schoffelen J-M (2016) A tutorial review of functional connectivity analysis methods and their interpretational pitfalls. *Front Syst Neurosci* 9:175.
15. Hagoort P (2013) MUC (Memory, Unification, Control) and beyond. *Front Psychol* 4:416.
16. Peelen MV, Caramazza A (2012) Conceptual object representations in human anterior temporal cortex. *J Neurosci* 32:15728–15736.
17. Rice GE, Lambon Ralph MA, Hoffman P (2015) The roles of left versus right anterior temporal lobes in conceptual knowledge: An ALE meta-analysis of 97 functional neuroimaging studies. *Cereb Cortex* 25:4374–4391.
18. Dronkers NF, Wilkins DP, Van Valin RD, Jr, Redfern BB, Jaeger JJ (2004) Lesion analysis of the brain areas involved in language comprehension. *Cognition* 92:145–177.
19. Turken AU, Dronkers NF (2011) The neural architecture of the language comprehension network: Converging evidence from lesion and connectivity analyses. *Front Syst Neurosci* 5:1–20.
20. Vigneau M, et al. (2011) What is right-hemisphere contribution to phonological, lexico-semantic, and sentence processing? Insights from a meta-analysis. *Neuroimage* 54:577–593.
21. Markov NT, et al. (2014) Anatomy of hierarchy: Feedforward and feedback pathways in macaque visual cortex. *J Comp Neurol* 522:225–259.
22. van Kerkoerle T, et al. (2014) Alpha and gamma oscillations characterize feedback and feedforward processing in monkey visual cortex. *Proc Natl Acad Sci USA* 111:14332–14341.
23. Lam NHL, Schoffelen J-M, Uddén J, Hultén A, Hagoort P (2016) Neural activity during sentence processing as reflected in theta, alpha, beta, and gamma oscillations. *Neuroimage* 142:43–54.
24. Ercsey-Ravasz M, et al. (2013) A predictive network model of cerebral cortical connectivity based on a distance rule. *Neuron* 80:184–197.
25. Siegel M, Donner TH, Engel AK (2012) Spectral fingerprints of large-scale neuronal interactions. *Nat Rev Neurosci* 13:121–134.
26. Stolk A, Todorovic A, Schoffelen J-M, Oostenveld R (2013) Online and offline tools for head movement compensation in MEG. *Neuroimage* 68:39–48.
27. Oostenveld R, Fries P, Maris E, Schoffelen J-M (2011) FieldTrip: Open source software for advanced analysis of MEG, EEG, and invasive electrophysiological data. *Comput Intell Neurosci* 2011:156869.
28. Xu L, et al. (2009) ASEO: A method for the simultaneous estimation of single-trial event-related potentials and ongoing brain activities. *IEEE Trans Biomed Eng* 56:111–121.
29. Wang X, Chen Y, Ding M (2008) Estimating Granger causality after stimulus onset: A cautionary note. *Neuroimage* 41:767–776.
30. Särelä J, Valpola H (2005) Denoising source separation. *J Mach Learn Res* 6:233–272.
31. Wang X, Ding M (2011) Relation between P300 and event-related theta-band synchronization: A single-trial analysis. *Clin Neurophysiol* 122:916–924.
32. Van Veen BD, van Drongelen W, Yuchtman M, Suzuki A (1997) Localization of brain electrical activity via linearly constrained minimum variance spatial filtering. *IEEE Trans Biomed Eng* 44:867–880.
33. Markov NT, et al. (2014) A weighted and directed interareal connectivity matrix for macaque cerebral cortex. *Cereb Cortex* 24:17–36.
34. Dhamala M, Rangarajan G, Ding M (2008) Analyzing information flow in brain networks with nonparametric Granger causality. *Neuroimage* 41:354–362.
35. Wang X, Chen Y, Bressler SL, Ding M (2007) Granger causality between multiple interdependent neurobiological time series: Blockwise versus pairwise methods. *Int J Neural Syst* 17:71–78.
36. Haufe S, Nikulin VV, Müller K-R, Nolte G (2013) A critical assessment of connectivity measures for EEG data: A simulation study. *Neuroimage* 64:120–133.
37. Vinck M, et al. (2015) How to detect the Granger-causal flow direction in the presence of additive noise? *Neuroimage* 108:301–318.
38. Li Y, Ngom A (2013) The non-negative matrix factorization toolbox for biological data mining. *Source Code Biol Med* 8:10.
39. Ghanbari Y, Bloy L, Batmanghelich K, Roberts TPL, Verma R (2012) Dominant component analysis of electrophysiological connectivity networks. *Medical Image Computing and Computer-Assisted Intervention – MICCAI 2012*. Lecture Notes in Computer Science, eds Ayache N, Delingette H, Golland P, Mori K (Springer, New York), pp 231–238.
40. Himberg J, Hyvärinen A (2003) Icasso: Software for investigating the reliability of ICA estimates by clustering and visualization. *2003 IEEE 13th Workshop on Neural Networks for Signal Processing* (IEEE, Piscataway, NJ), pp 259–268.
41. Nolte G (2003) The magnetic lead field theorem in the quasi-static approximation and its use for magnetoencephalography forward calculation in realistic volume conductors. *Phys Med Biol* 48:3637–3652.
42. Bosman CA, et al. (2012) Attentional stimulus selection through selective synchronization between monkey visual areas. *Neuron* 75:875–888.
43. Kim J, Park H (2008) Sparse nonnegative matrix factorization for clustering (Georgia Institute of Technology, Atlanta).
44. Ding C, He X, Simon HD (2014) On the equivalence of nonnegative matrix factorization and spectral clustering. *Proceedings of the 2005 SIAM International Conference on Data Mining* (Society for Industrial and Applied Mathematics, Philadelphia), pp 606–610.